Analytical Methods for the Extraction of Solar-Cell Single- and Double-Diode Model Parameters from *I–V* Characteristics

DANIEL S. H. CHAN, MEMBER, IEEE, AND JACOB C. H. PHANG, MEMBER, IEEE

Abstract—**Analytical solutions for the rapid extraction of single- and double-diode model parameters from experimental data are described. The resulting parameters' values are shown to have less than 10 percent error for most solar cells. Error contours are also illustrated to define the range of validity of these methods.**

I. Introduction

THE USE OF lumped circuit models is a convenient and widely used method for simulating solar-cell performance. There are currently two main lumped circuit models in use. The first one is the single-diode model described by the modified Shockley diode equation incorporating a diode quality factor to account for the effect of recombination in the space-charge region. Analytical expressions for the rapid extraction of parameters for this model were recently reported [1]. The second model, commonly referred to as the double-diode model, simulates the space-charge recombination effect by incorporating a separate current component with its own exponential voltage dependence. The double-diode model has been shown to be a more accurate representation of solar cell behavior than the single-diode model [2]. The single-diode model is particularly inaccurate in describing cell behavior at low illuminations. Recent work has also shown that fitting the single-diode model to cell characteristics collected at low illuminations can result in negative series resistance values [3], while even at higher illuminations up to one sun, the use of the single-diode model can result in significantly different series resistance values [4].

However, these circuit models (see Fig. 1) are based on assumptions that may not always be valid. The main assumption is that of linearity, namely that the current flowing through the cell is a superposition of two currents, one due to junction bias and the other due to illumination. This main assumption is made possible by other simplifying assumptions. For example, the material parameters are assumed to be insensitive to changes in either bias or illumination, and the minority-carrier concentrations at the edges of the space-charge regions are assumed to be dependent on the junction bias and independent of illumination. These assumptions may not be accurate. However, these models do generally fit experimental *I–V* characteristics fairly accurately, and can provide a very useful tool in assessing cell performance provided the model parameters are easily obtainable. For example, model parameters may be used for solar-cell design by optimizing the parameters for best performance, especially if these can be closely associated with fabrication process parameters. The model parameters can also be a useful tool for monitoring solar-cell manufacturing processes if the parameter values can be determined simply and rapidly.

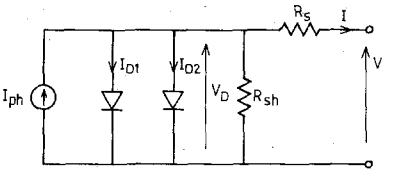

Fig. 1. The double-diode solar-cell model.

Current methods for extracting model parameters generally require curve fitting or some other iterative procedure. This paper describes two analytical solutions for the extraction of double-diode model parameters from measurements of cell characteristics. These methods were applied to various types of cells with differing quality. The error contours defining the region of validity of the double-diode analytical expressions together with full error contours for the previously reported single-diode analytical expressions [1] are also presented and discussed. It is demonstrated that the various analytical solutions can together make a significant contribution to the rapid extraction of solar-cell parameters.

II. Analytical Extraction Methods

A. Single-Diode Model

The single-diode model assumes that the dark current can be described by a single exponential dependence modified by the diode ideality factor n. Thus, the current–voltage relationship is given by

$$I = I_{ph} - \frac{V + IR_s}{R_{sh}} - I_s\left(\exp\frac{V + IR_s}{nV_T} - 1\right) \quad (1)$$

Manuscript received June 2, 1986; revised September 2, 1986.

The authors are with the Department of Electrical Engineering, National University of Singapore, Kent Ridge, Singapore 0511.

IEEE Log Number 8611467.

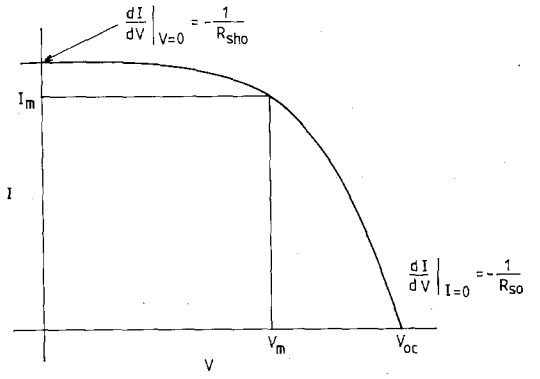

Fig. 2. Input parameters from I–V characteristics.

where

I_{ph} is the photocurrent (in amperes),
I_s is the diode saturation current (in amperes),
n is the diode quality factor,
R_s is the lumped series resistance (in ohms),
R_{sh} is the lumped shunt resistance (in ohms), and
V_T kT/q.

Analytical expressions for the extraction of the model parameters have been described elsewhere [1] and are reproduced here for completeness.

$$n = \frac{V_m + I_m R_{s0} - V_{oc}}{V_T\left\{\ln\left(I_{sc} - \frac{V_m}{R_{sh0}} - I_m\right) - \ln\left(I_{sc} - \frac{V_{oc}}{R_{sh}}\right) + \frac{I_m}{I_{sc} - (V_{oc}/R_{sh0})}\right\}} \tag{2}$$

$$I_s = \left(I_{sc} - \frac{V_{oc}}{R_{sh}}\right)\exp\left(\frac{-V_{oc}}{nV_T}\right) \tag{3}$$

$$R_s = R_{s0} - \frac{nV_T}{I_s}\exp\left(\frac{-V_{oc}}{nV_T}\right) \tag{4}$$

$$R_{sh} = R_{sh0} \tag{5}$$

$$I_{ph} = I_{sc}\left(1 + \frac{R_s}{R_{sh}}\right) + I_s\left(\exp\frac{I_{sc}R_s}{nV_T} - 1\right) \tag{6}$$

where V_{oc}, I_{sc}, V_m, I_m, R_{s0}, and R_{sh0} are the input parameters defined in Fig. 2.

B. Double-Diode Model

The double-diode model of a solar cell is given in Fig. 1. At a given illumination, the current–voltage relationship is given by

$$I = I_{ph} - I_{s1}\left(\exp\frac{V + IR_s}{V_T} - 1\right) - I_{s2}\left(\exp\frac{V + IR_s}{2V_T} - 1\right) - \frac{V + IR_s}{R_{sh}}. \tag{7}$$

It will be shown that the circuit parameters I_{ph}, I_{s1}, I_{s2}, R_s, and R_{sh} at a particular temperature and illumination can be computed from the values V_{oc}, I_{sc}, V_m, I_m, R_{s0}, and R_{sh0} measured from the I–V characteristic as shown in Fig. 2.

At the short circuit point, $V = 0$, $I = I_{sc}$ gives

$$I_{sc} = I_{ph} - I_{s1}\left(\exp\frac{I_{sc}R_s}{V_T} - 1\right) - I_{s2}\left(\exp\frac{I_{sc}R_s}{2V_T} - 1\right) - \frac{I_{sc}R_s}{R_{sh}}. \tag{8}$$

At the open circuit point $V = V_{oc}$, $I = 0$, we have

$$I_{ph} = I_{s1}\left(\exp\frac{V_{oc}}{V_T} - 1\right) + I_{s2}\left(\exp\frac{V_{oc}}{2V_T} - 1\right) + \frac{V_{oc}}{R_{sh}}. \tag{9}$$

Eliminating I_{ph} gives

$$I_{sc} = I_{s1}\left(\exp\frac{V_{oc}}{V_T} - \exp\frac{I_{sc}R_s}{V_T}\right) + I_{s2}\left(\exp\frac{V_{oc}}{2V_T} - \exp\frac{I_{sc}R_s}{2V_T}\right) + \frac{V_{oc} - I_{sc}R_s}{R_{sh}}. \tag{10}$$

Differentiating (7) with respect to I gives

$$-\frac{dV}{dI}\left(\frac{I_{s1}}{V_T}\exp\frac{V + IR_s}{V_T} + \frac{I_{s2}}{2V_T}\exp\frac{V + IR_s}{2V_T} + \frac{1}{R_{sh}}\right) = 1 + \frac{I_{s1}R_s}{V_T}\exp\frac{V + IR_s}{V_T} + \frac{I_{s2}R_s}{2V_T}\exp\frac{V + IR_s}{2V_T} + \frac{R_s}{R_{sh}}. \tag{11}$$

At the open circuit point, $I = 0$, $V = V_{oc}$, $-(dV/dI) = R_{s0}$; therefore

$$(R_{s0} - R_s)\left(\frac{I_{s1}}{V_T}\exp\frac{V_{oc}}{V_T} + \frac{I_{s2}}{2V_T}\exp\frac{V_{oc}}{2V_T} + \frac{1}{R_{sh}}\right) - 1 = 0. \tag{12}$$

At the short circuit point, $V = 0$, $I = I_{sc}$, $-(dV/dI) = R_{sh0}$

$$(R_{sh0} - R_s)\left(\frac{I_{s1}}{V_T}\exp\frac{I_{sc}R_s}{V_T} + \frac{I_{s2}}{2V_T}\exp\frac{I_{sc}R_s}{2V_T} + \frac{1}{R_{sh}}\right) - 1 = 0. \tag{13}$$

Substituting the maximum power point values $I = I_m$ and $V = V_m$ into (7) and using I_{ph} from (9) gives

$$I_m\left(1 + \frac{R_s}{R_{sh}}\right) = I_{s1}\left(\exp\frac{V_{oc}}{V_T} - \exp\frac{V_m + I_mR_s}{V_T}\right) + I_{s2}\left(\exp\frac{V_{oc}}{2V_T} - \exp\frac{V_m + I_mR_s}{2V_T}\right) + \frac{V_{oc} - V_m}{R_{sh}}. \quad (14)$$

I_{s1}, I_{s2}, R_s, and R_{sh} can be determined by solving (10), (12), (13), and (14) with the Newton–Raphson method. I_{ph} can be evaluated from (9). However, this method requires extensive computation and also good initial guesses for the iterations to converge. The analysis below shows a method whereby analytical solutions of the required parameters may be obtained.

For most cells under AM1 illumination, the following approximations may be made:

$$\exp\frac{V_{oc}}{nV_T} \gg \exp\frac{I_{sc}R_s}{nV_T}, \quad \text{where} \quad n = 1 \text{ or } 2 \quad (15)$$

$$R_{sh}, R_{sh0} \gg R_s \quad (16)$$

$$\frac{I_{s1}}{V_T}\exp\frac{I_{sc}R_s}{V_T}, \frac{I_{s2}}{2V_T}\exp\frac{I_{sc}R_s}{2V_T} \ll \frac{I}{R_{sh0}} \text{ and } I_{sc}R_s \ll V_{0c}. \quad (17)$$

Equations (10), (12), (14), and (13) become, respectively,

$$I_{s1}\exp\frac{V_{oc}}{V_T} + I_{s2}\exp\frac{V_{oc}}{2V_T} - I_{sc} + \frac{V_{oc}}{R_{sh}} = 0 \quad (18)$$

$$(R_{s0} - R_s)\left(\frac{I_{s1}}{V_T}\exp\frac{V_{oc}}{V_T} + \frac{I_{s2}}{2V_T}\exp\frac{V_{oc}}{2V_T}\right) - 1 = 0 \quad (19)$$

$$I_{s1}\exp\frac{V_{oc}}{V_T} + I_{s2}\exp\frac{V_{oc}}{2V_T} - I_{s1}\exp\frac{V_m + I_mR_s}{V_T} - I_{s2}\exp\frac{V_m + I_mR_s}{2V_T} + \frac{V_{oc} - V_m}{R_{sh}} - I_m = 0 \quad (20)$$

$$R_{sh} = R_{sh0}. \quad (21)$$

By eliminating I_{s1} and I_{s2} from (18)–(20) and using (21), a nonlinear equation in R_s in terms of the measured parameters is

$$I_{sc} - I_m - \frac{V_m}{R_{sh0}} - \left(\frac{V_{oc}}{R_{sh0}} - I_{sc} + \frac{2V_T}{R_{s0} - R_s}\right)\exp\frac{V_m - V_{oc}}{V_T}\exp\frac{I_mR_s}{V_T} - 2\left(I_{sc} - \frac{V_{oc}}{R_{sh0}} - \frac{V_T}{R_{s0} - R_s}\right)\exp\frac{V_m - V_{oc}}{2V_T}\exp\frac{I_mR_s}{2V_T} = 0. \quad (22)$$

1) Quadratic Solution of R_s: By making an approximation as follows:

$$\exp(kR_s) = 1 + kR_s \quad (23)$$

for

$$k = \frac{I_m}{V_T} \text{ and } \frac{I_m}{2V_T}$$

and defining the new symbols

$$\alpha = I_{sc} - \frac{V_{oc}}{R_{sh0}} \quad (24)$$

$$\beta = I_{sc} - I_m - \frac{V_m}{R_{sh0}} \quad (25)$$

$$\gamma = \exp\left(\frac{V_m - V_{oc}}{2V_T}\right) \quad (26)$$

$$\delta = \frac{I_m}{V_T} \quad (27)$$

the following quadratic equation in R_s may be obtained:

$$aR_s^2 + bR_s + c = 0 \quad (28)$$

where

$$a = \alpha\gamma\delta(1 - \gamma) \quad (29)$$

$$b = \alpha\gamma(2 - \gamma) + \alpha\gamma\delta R_{s0}(\gamma - 1) - \beta + \gamma\delta V_T(1 - 2\gamma) \quad (30)$$

$$c = \alpha\gamma R_{s0}(\gamma - 2) + \beta R_{s0} + 2\gamma V_T(1 - \gamma). \quad (31)$$

R_s can then be obtained by the solution to the quadratic equation as follows:

$$R_s = \frac{-b \pm \sqrt{b^2 - 4ac}}{2a}. \quad (32)$$

2) Cubic Solution of R_s: A more accurate solution may be obtained by including one more term in (23), i.e.,

$$\exp(kR_s) = 1 + kR_s + \frac{k^2R_s^2}{2} \quad (33)$$

for

$$k = \frac{I_m}{V_T} \text{ and } \frac{I_m}{2V_T}.$$

The resultant cubic equation in R_s is

$$AR_s^3 + BR_s^2 + CR_s + D = 0 \quad (34)$$

where

$$A = \alpha\gamma\delta^2(1 - 2\gamma) \quad (35)$$

$$B = 4\alpha\gamma\delta(1 - \gamma) + \alpha\gamma\delta^2R_{s0}(2\gamma - 1) + \gamma\delta^2V_T(1 - 4\gamma) \quad (36)$$

$$C = 4\alpha\gamma(2 - \gamma) + 4\alpha\gamma\delta R_{s0}(\gamma - 1) + 4\gamma\delta V_T(1 - 2\gamma) - 4\beta \quad (37)$$

$$D = 4\alpha\gamma R_{s0}(\gamma - 2) + 8\gamma V_T(1 - \gamma) + 4\beta R_{s0}. \quad (38)$$

TABLE I
A COMPARISON BETWEEN RESULTS OBTAINED FROM THE ACCURATE, QUADRATIC, AND CUBIC SOLUTIONS TO THE DOUBLE-DIODE MODEL FOR THREE CELLS

Experimental Results	Cell CN1-500-50			Cell SG1-770-50			Cell TL1-900-50		
V_{oc} (V)	0.5327			0.5094			0.5317		
I_{sc} (A)	0.5341			0.7767			0.9058		
V_m (V)	0.4446			0.4131			0.4137		
I_m (A)	0.4677			0.6979			0.7939		
R_{so} (Ω)	0.0698			0.060			0.0719		
R_{sho} (Ω)	21.8			142.0			19.62		
T (°C)	50			50			50		
Results	Accurate Solution	Quadratic Solution (% diff)	Cubic Solution (% diff)	Accurate Solution	Quadratic Solution (% diff)	Cubic Solution (% diff)	Accurate Solution	Quadratic Solution (% diff)	Cubic Solution (% diff)
I_{ph} (A)	0.5343	0.5340 (-0.052)	0.5340 (-0.052)	0.7767	0.7763 (-0.054)	0.7764 (-0.051)	0.9072	0.9053 (-0.214)	0.9054 (-0.207)
I_{s1} (nA)	1.888	1.879 (-0.48)	1.885 (-0.14)	6.289	6.047 (-3.84)	6.269 (-0.32)	2.466	2.059 (-16.532)	2.383 (-3.40)
I_{s2} (μA)	8.885	8.993 (1.22)	8.903 (0.21)	23.35	25.584 (9.54)	23.502 (0.63)	28.31	33.892 (19.699)	29.355 (3.67)
R_s (mΩ)	7.630	7.305 (-4.25)	7.396 (-3.07)	18.06	17.354 (-3.92)	17.983 (-0.44)	31.17	28.479 (-8.627)	30.529 (-2.05)
R_{sh} (Ω)	21.874	21.875 (0.005)	21.874 (-0.001)	153.77	154.86 (0.71)	153.83 (0.043)	19.92	19.970 (0.259)	19.928 (0.047)

Analytical solutions for cubic equations have been described in [5] and are summarized in the Appendix.

3) I_{s1}, I_{s2}, R_{sh}, and I_{ph}: From (18) and (19)

$$I_{s1} = \left(\frac{V_{oc}}{R_{sh0}} - I_{sc} + \frac{2V_T}{R_{s0} - R_s}\right) \exp - \left(\frac{V_{oc}}{V_T}\right) \tag{39}$$

$$I_{s2} = 2\left(I_{sc} - \frac{V_{oc}}{R_{sh0}} - \frac{V_T}{R_{s0} - R_s}\right) \exp - \left(\frac{V_{oc}}{2V_T}\right). \tag{40}$$

From (13)

$$R_{sh} = \left\{\frac{1}{R_{sh0} - R_s} - \frac{I_{s1}}{V_T} \exp \frac{I_{sc}R_s}{V_T} - \frac{I_{s2}}{2V_T} \exp \frac{I_{sc}R_s}{2V_T}\right\}^{-1}. \tag{41}$$

From (9)

$$I_{ph} = I_{s1}\left(\exp \frac{V_{oc}}{V_T} - 1\right) + I_{s2}\left(\exp \frac{V_{oc}}{2V_T} - 1\right) + \frac{V_{oc}}{R_{sh}}. \tag{42}$$

Thus by finding a value for R_s by either the quadratic or cubic solutions, the other four parameters can also be recovered.

III. RESULTS

The model parameters of three cells from different manufacturers were extracted using the double-diode analytical methods of solutions and the results are in Table I. Cell *CN*1 is a 2-in-diameter concentrator cell and *SG*1 and *TL*1 are normal 3-in silicon cells of differing quality. All three cells were illuminated under *AM*1 conditions and the experimental parameters were determined in a computer controlled measurement system that has been described earlier [6]. The accurate solutions were obtained by solving (10), (12), (13), and (14) iteratively by the Newton–Raphson method. As expected, the errors in the parameter values obtained from the quadratic solution are much higher than that from the cubic solution. For the quadratic solution, the greatest errors are in I_{s2}, which could be as high as 19.7 percent as in cell *TL*1, whereas the errors from the cubic solution are all within 4 percent.

The results presented in Table I are representative of those obtained by applying the quadratic and cubic solutions to sets of experimental data from different cells. Our experience in applying the cubic expressions to experimental data has been that the numerical solution had, in most cases, one real and two complex roots. In the remaining cases, the solution gave three real roots, only one of which was positive. The situation of multiple or zero positive real roots was seldom encountered.

IV. ERROR CONTOURS

The errors in the various analytical solutions were computed by generating a theoretical *I–V* characteristic using a set of parameter values and subsequently recovering the parameters using the analytical expressions. The recovered values were then compared with the starting values to obtain percentage errors. In order to assess how the errors varied with different types of cells under different conditions, the error computations were carried out for different combinations of starting values.

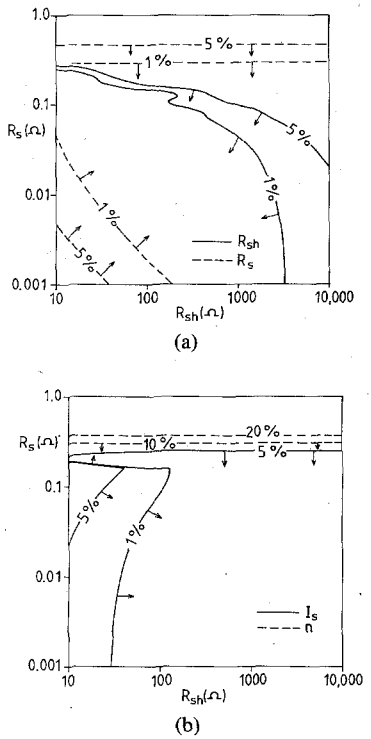

Fig. 3. Error contours of (a) R_s, R_{sh}; (b) I_s, n; for single-diode analytical solution with $I_{ph} = 1$ A, $I_s = 10^{-7}$ A, $n = 1.3$.

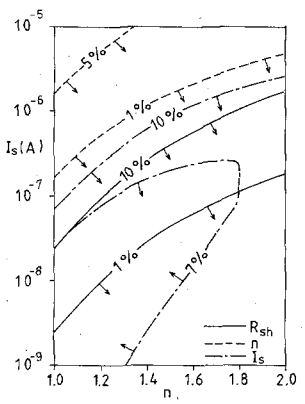

Fig. 4. Error contours of n, I_s, R_{sh} for single-diode analytical solution with $I_{ph} = 1$ A, $R_s = 0.2\ \Omega$, $R_{sh} = 100\ \Omega$.

A. Single-Diode Analytical Expressions

Errors in the single-diode expressions were first computed using base values of $I_{ph} = 1$ A, $I_s = 10^{-7}$ A, $n = 1.3$, and different combinations of R_s (from 1 mΩ to 1 Ω) and R_{sh} (from 10 Ω to 10 kΩ). The errors for each parameter were plotted in a $R_s - R_{sh}$ grid, shown in Fig. 3(a) and (b). Errors were also computed for base values of $I_{ph} = 1$ A, $R_s = 0.2\ \Omega$, $R_{sh} = 100\ \Omega$, and different combinations of I_s (from 10^{-9} to 10^{-5} A), and n (1.0 to 2.0), and the errors in n, I_s, and R_{sh}, are contoured in Fig. 4. The errors in R_s for these parameter base values were found to be insignificant and thus not plotted. In all these contour plots, the arrow directions point toward decreasing absolute percentage values.

It can be seen from Fig. 3(a) and (b) that for the base values of n, I_s, and I_{ph} used, the accuracy of the expressions are not strongly sensitive to the value of R_{sh} provided R_{sh} is greater than 10 Ω, and are limited largely by the value of R_s, and that acceptable accuracy can be obtained for all parameters if R_s is less than 200 mΩ. The errors increase rapidly when R_s is greater than 200 mΩ.

For the second part of the error plots (Fig. 4), different base values of R_s and R_{sh} were also attempted, and it was found that errors were below 1 percent for the ranges of n and I_s investigated provided R_s was below 150 mΩ. In order to explore the limits of the method, a higher R_s base value was chosen, and therefore, I_{ph}, R_s, and R_{sh} values of 1 A, 200 mΩ, and 100 Ω, respectively, were used as base values. The resulting plots in Fig. 4 show that with such high values of R_s and I_{ph}, the expressions are more accurate for low I_s and high n values.

The combined error plots (Figs. 3 and 4) show that at $I_{ph} = 1$ A the analytical expressions are applicable provided $R_s < 150$ mΩ. Since these errors were largely incurred by neglecting some exp $(I_{sc}R_s/nV_t)$ terms in the derivation of the analytical expressions [1], we can expect the upper limit of R_s to increase beyond 150 mΩ at lower illuminations. This fact considerably widens the range of applicability of these analytical expressions.

B. Double-Diode Analytical Expressions

Errors for the double-diode expressions were first computed using base values of $I_{ph} = 1$ A, $I_{s1} = 10^{-9}$ A, $I_{s2} = 10^{-5}$ A, while R_s and R_{sh} values were varied from 1 mΩ to 1 Ω and 10 Ω to 10 kΩ, respectively. The percentage errors were then plotted in a grid of R_s and R_{sh} and contoured. Secondly, using base values of $I_{ph} = 1$ A, $R_s = 10$ mΩ, and $R_{sh} = 100\ \Omega$, I_{s1} and I_{s2} were varied between 10^{-12} and 10^{-7} A and 10^{-7} and 10^{-4} A, respectively. The magnitude of the percentage errors were then plotted in a grid of I_{s1} and I_{s2}. The value of I_{ph} selected corresponds to around $AM1$ for a 3-in cell.

1) Quadratic Case: The errors for the quadratic analytical solution were computed in the manner described above and are plotted in Figs. 5 and 6. Fig. 5(a) shows the 1- and 10-percent absolute percentage error contours for R_s and R_{sh} in a $R_s - R_{sh}$ grid while Fig. 5(b) gives the same error contours for I_{ph}, I_{s1}, and I_{s2}. These plots show that the factor limiting the accuracy of the analytical solution is the value of R_s that should not exceed about 50 mΩ if the four parameters I_{ph}, I_{s1}, R_s, and R_{sh} are to have errors of less than 10 percent, although under these conditions the error of the I_{s2} value would be slightly higher. In fact, it can be observed from (23) that the accuracy of the solution is largely dependent on the value of I_mR_s. Thus, the accuracy of the extracted parameters would deteriorate significantly for illumination levels higher than $AM1$ and R_s greater than about 50 mΩ. This situation, however, does not seriously limit the application of this solution as most cells operating at high illuminations have low series resistances.

The absolute percentage errors of the quadratic solution plotted in a $I_{s1} - I_{s2}$ grid are shown in Fig. 6. For all five parameters, there is a 10-percent contour running diago-

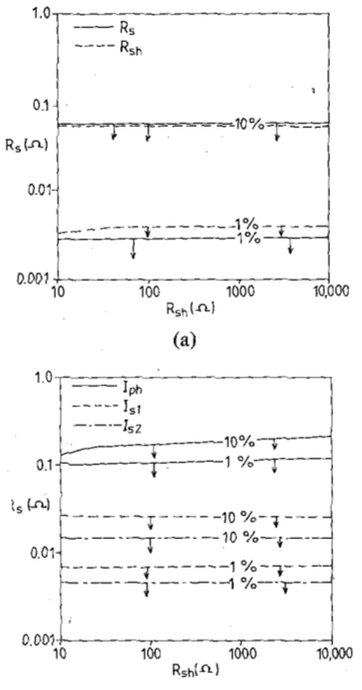

Fig. 5. Error contours of (a) R_s and R_{sh}; (b) I_{ph}, I_{s1}, I_{s2}; for double-diode quadratic solution with $I_{ph} = 1$ A, $I_{s1} = 10^{-9}$ A, $I_{s2} = 10^{-5}$ A.

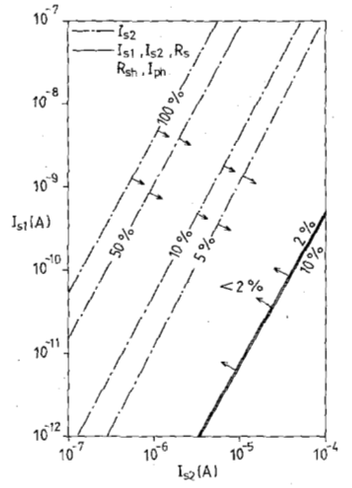

Fig. 6. Error contours of I_{s1}, I_{s2}, R_s, and R_{sh} for double-diode quadratic solution with $I_{ph} = 1$ A, $R_s = 10$ mΩ, $R_{sh} = 100$ Ω.

nally along the lower right-hand side of the plot. The errors mount up rapidly to the right of this contour, and the quadratic solution fails in this region. For I_{s2}, however, there are additional diagonal contours in the top left-hand region of the plot with the errors increasing to the left of these diagonals. Thus these two error constraints leave a diagonal band defining the region of validity of the quadratic solution.

In order to appreciate the limitations of this method better, the equivalent value of the quality factor n from the single-diode model was computed from the I–V characteristics generated by the two-diode model for each set of parameters. These values were computed by an iterative

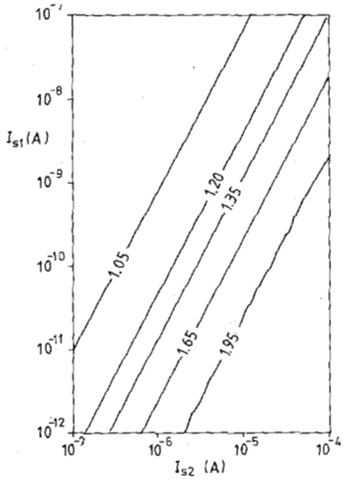

Fig. 7. Corresponding quality factor values from single-diode model with $I_{ph} = 1$ A, $R_s = 10$ mΩ, $R_{sh} = 100$ Ω.

method using the first guess values provided by the analytical solution (2)–(6) to the one-diode method. The results are plotted in Fig. 7. A comparison of Figs. 6 and 7 shows that the region of validity of the quadratic solution as defined by the 10-percent contours corresponds to n having values between 1.20 and 2.0. This gives an insight into the cause of the failure of the method. At n close to unity, the I_{s2} current component is insignificant compared to the I_{s1} component, thus making it difficult to extract I_{s2} accurately. The inverse situation applies for n close to 2. However, if the value of n was close to either 1 or 2, the single-diode model would be an appropriate description of cell performance and there would be little need for the double-diode model.

2) Cubic Case: The contours of the absolute percentage errors for the cubic case are presented in Figs. 8 and 9. It can be noted from Fig. 8(a) and (b) that the accuracy of the cubic solution is also determined by the value of R_s. As expected, this accuracy is a significant improvement over that of the quadratic solution. The errors in I_{s2} are somewhat larger than that for the other parameters. Thus R_s can be determined to 10-percent accuracy even if the series resistance was 100 mΩ, while I_{s2} could have the same accuracy if R_s was 30 mΩ.

Errors in R_s, R_{sh}, and I_{ph} were negligible for the base values used in computing Fig. 9. However, errors in I_{s1} and I_{s2} are given in Fig. 9, and this shows that the band of validity of the method has significantly widened as compared with the quadratic solution. A comparison of Fig. 9 with Fig. 7 shows that for the base values of I_{ph}, R_s, and R_{sh} used, the band of validity bounded by the 10-percent contours in I_{s1} and I_{s2} translates to n between 1.04 and 1.95. As in the quadratic solution, the same argument can be put forward, but now more strongly, that in cases where $n < 1.04$ or $n > 1.95$, the single-diode model can be a valid representation of diode behavior.

V. Conclusions

Analytical solutions for the extraction of parameters of the double-diode model have been presented. It has been

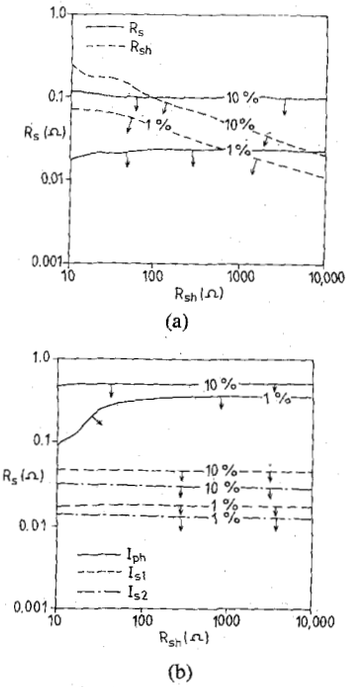

Fig. 8. Error contours of (a) R_s, R_{sh}; (b) I_{ph}, I_{s1}, I_{s2} for double-diode cubic solution with $I_{ph} = 1$ A, $I_{s1} = 10^{-9}$ A, $I_{s2} = 10^{-5}$ A.

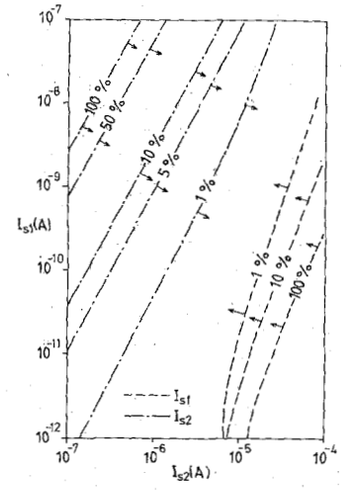

Fig. 9. Error contours of I_{s1} and I_{s2} for double-diode cubic solutions with $I_{ph} = 1$ A, $R_s = 10$ mΩ, $R_{sh} = 100$ Ω.

shown that the solutions have a wide range of validity provided the series resistance and illuminations are not both high. The error contours of the one-diode analytical solution have also been presented, and these show that this solution is accurate for R_s less than 200 mΩ at $I_{ph} = 1$ A. The analytical solutions presented here for both diode models complement each other and together greatly facilitate the rapid determination of lumped circuit model parameters of solar cells.

Appendix
Roots of Cubic Equations

$$Ax^3 + Bx^2 + Cx + D = 0. \tag{A1}$$

Substitute for

$$x = y - \frac{B}{3A} \tag{A2}$$

into (A1) gives

$$y^3 + py + q = 0 \tag{A3}$$

where

$$p = \frac{1}{3}\left[3\left(\frac{C}{A}\right) - \left(\frac{B}{A}\right)^2\right] \tag{A4}$$

$$q = \frac{1}{27}\left[2\left(\frac{B}{A}\right)^3 - 9\left(\frac{B}{A}\right)\left(\frac{C}{A}\right) + 27\left(\frac{D}{A}\right)\right]. \tag{A5}$$

For real values of A, B, C, and D, the nature of the solutions are determined by the parameters Δ as follows:

$$\Delta = \left(\frac{p}{3}\right)^3 + \left(\frac{q}{2}\right)^2 \tag{A6}$$

$\Delta > 0$ one real and two conjugate complex roots (A7)

$\Delta = 0$ 3 real roots at least two of which are equal (A8)

$\Delta < 0$ 3 real unequal roots. (A9)

The solutions are then given by

$$x_1 = u + v - \frac{B}{3A} \tag{A10}$$

$$x_2 = -\frac{u+v}{2} - \frac{B}{3A} + \frac{u-v}{2} i\sqrt{3} \tag{A11}$$

$$x_3 = -\frac{u+v}{2} - \frac{B}{3A} - \frac{u-v}{2} i\sqrt{3} \tag{A12}$$

where

$$u = \sqrt[3]{\frac{-q}{2} + \sqrt{\Delta}} \tag{A13}$$

$$v = \sqrt[3]{\frac{-q}{2} - \sqrt{\Delta}}. \tag{A14}$$

If $\Delta < 0$, the solutions can be expressed in trigonometric form as follows:

$$x_1 = -\frac{B}{3A} + 2\sqrt{\frac{|p|}{3}} \cos\frac{\phi}{3} \tag{A15}$$

$$x_2 = -\frac{B}{3A} - 2\sqrt{\frac{|p|}{3}} \cos\frac{\phi + \pi}{3} \tag{A16}$$

$$x_3 = -\frac{B}{3A} - 2\sqrt{\frac{|p|}{3}} \cos\frac{\phi - \pi}{3} \tag{A17}$$

where

$$\phi = \cos^{-1}\frac{-q/2}{\sqrt{|p|^3/27}}.$$

REFERENCES

[1] J. C. H. Phang, D. S. H. Chan, and J. R. Phillips, "Accurate analytical method for the extraction of solar cell model parameters," *Electron. Lett.*, vol. 20, no. 10, pp. 406–408, 1984.

[2] M. Wolf, G. J. Noel, and R. J. Stirn, "Investigation of the double exponential in the current–voltage characteristics of silicon solar cells," *IEEE Trans. Electron Devices*, vol. ED-24, pp. 419–428, 1977.

[3] D. S. H. Chan, J. C. H. Phang, J. R. Phillips, and M. S. Loong, "A comparison of extracted solar cell parameters from single and double lumped circuit models," in *Tech. Dig. 1st Int. Photovoltaic Science and Engineering Conf.* (Kobe, Japan), pp. 151–153, Nov. 13–16, 1984.

[4] J. P. Charles, I. Mekkaoui-Alaoui, G. Bordure, and P. Mialhe, "A critical study of the effectiveness of the single and double exponential models for the *I–V* characterisation of solar cells," *Solid-State Electron.*, vol. 28, pp. 807–820, 1985.

[5] J. V. Upensky, *Theory of Equations*. New York: McGraw-Hill, 1948.

[6] D. S. H. Chan, J. R. Phillips, and J. C. H. Phang, "A comparative study of extraction methods for solar cell model parameters," *Solid-State Electron.*, vol. 29, no. 3, pp. 329–337, 1986.

Daniel S. H. Chan (M'79) was born in Hong Kong on May 22, 1948. He received the B.Sc. and M.Sc. degrees from the University of Manchester Institute of Science and Technology, and the Ph.D. degree from the University of Salford in 1975.

He joined the Electrical Engineering Department at the National University of Singapore in 1980, where he is now a Senior Lecturer. His present research interests are in photovoltaic devices and in the application of the SEM to failure analysis of integrated circuits.

*

Jacob C. H. Phang (M'81) was born in Singapore on October 6, 1953. He received the B.A. and Ph.D. degrees from Cambridge University in 1975 and 1979, respectively.

He then joined the Electrical Engineering Department of the National University of Singapore where he is now a Senior Lecturer. His research interests are in solar cell evaluation techniques and scanning electron microscopy applied to the failure analysis of integrated circuits.